Biointerface Research in Applied Chemistry
Open-Access Journal (ISSN: 2069-5837)

Article
Volume 14, Issue 1, 2024, 6
https://doi.org/10.33263/BRIAC141.006

Opto-Electrochemical Sensing of MDMA Molecule Through a Nanoarchitecture Formed Quantum Dots (QDs) Modified Aptasensor

Shringika Soni [1], Utkarsh Jain [2], Nidhi Chauhan [2,*]

[1] Amity Institute of Nanotechnology (AINT), Amity University Uttar Pradesh (AUUP), Noida-201313, India
[2] School of Health Sciences & Technology (SoHST), University of Petroleum and Energy Studies (UPES), Bidholi, Dehradun 248007, India
* Correspondence: nidhichauhan@rediffmail.com (N.C.);

Scopus Author ID 36909471600

Received: 20.04.2022; Accepted: 5.01.2023; Published: 2.02.2024

Abstract: This study designed a novel electrochemical aptasensor for single-step quantification of 3,4-methylenedioxymethamphetamine (MDMA) based proximity-based assay. This detection technique depends upon direct recognition of the target by a specific aptamer, a prerequisite by nitrogen-doped carbon dots (N-CDs) to enhance the sensitivity and thus induce the redox current at the modified electrode. The fabricated device reports the advantage of a label-free aptasensor for MDMA detection with an outstanding detection limit of 0.18 nM and sensitivity of 0.36 Ω/ nM in the linear range of 0.01 nM to 1.0 nM. Under potentially controlled conditions, developed aptasensors also exhibited their applicability in diluted spiked urine samples with a recovery rate in the range of 88-92%. Overall, the aptasensor can be a very useful and cost-effective tool for targeted MDMA detection in biological samples in the field of forensic science.

Keywords: aptamer; impedimetric sensor; MDMA; N-carbon dots; recreational drug.

1. Introduction

3,4-methylenedioxymethamphetamine (MDMA) is a highly addictive psychoactive compound, which was later also termed 'Ecstasy' by a Californian drug dealer to use recreationally [1,2]. It was characterized by a combination of hallucinogenic and stimulant properties to increase sales as a street drug. World Drug Report, Drugs, and Crime, United Nations estimated that approximately 271 million people are addicted to illicit drug consumption globally [3]; among them, 20 million people used 'ecstasy' in 2018 [4]. It is higher than the global average in the sub-region of Australia and New Zealand (2.8%), North America (0.9%), and Western and Central Europe (0.9%). However, it has also gained interest in adjunct psychotherapy for post-traumatic stress disorder (PTSD) and attention deficit hyperactivity disorder (ADHD) treatment [1,5]. But, due to extreme euphoric, hallucinogenic, auditory, or visual perceptions and its highly addictive nature, MDMA has questionable use in medical science [6,7].

Generally, gas chromatography (GC) and high-performance liquid chromatography (HPLC) in a combination of mass spectroscopy are used to determine MDMA in clinical samples [8–11]. However, these methods are expensive, time-consuming, and require heavy laboratory set-up and technical expertise to perform and analyze the samples [12–15]. On the

other hand, electrochemical sensors bases analysis possesses excellent characteristics, including easy process, low cost, rapid operation, easy miniaturization, and practicality [15–18]. To date, very limited electrochemical sensors have been developed for MDMA determination. For instance, *Tadini et al.* has designed a cucurbit[6]uril-modified electrochemical sensor to directly detect MDMA in the range of 3.5 μM [19]. The MDMA was captured by a cavity created by aromatic and heterocyclic rings moiety of CB[6] that oxidized to generate a delocalized cation over the aromatic ring. However, the high detection limit and insolubility in the water of CB[6] [20,21] limit their application in real-world analytics. Therefore, to improve the sensitivity of the sensing platform, a study published in *Electrochimica Acta* showed platinum nanoparticles (PtNPs)/ carbon nanohorns decorated electrochemical devices for MDMA detection [22]. This 3D nanocomposite demonstrated excellent electrocatalytic properties against the drug and reported 0.018 μM as a limit of detection (LOD). But, this study also exhibited a change in signals in the presence of morphine, thus limiting the sensor's selectivity. In the direction of improving the selectivity and stability of the system, *Couto et al.* designed molecularly imprinted poly(o-phenylenediamine) polymer-based impedimetric sensor for MDMA detection and reported a LOD of 0.79 μM [23], which is a relatively higher in analytical chemistry.

Considering the huge gap in sensing technology described above, research efforts have been dedicated to developing economical, reliable, and rapid on-spot devices. In this direction, aptamers are playing an important role in the field of small molecule detection, such as drugs such as cocaine [24,25], opioids [26,27], antibiotics [28–30], and metals [31,32]. Aptamers are small RNA or single-stranded DNA (ss-DNA) sequences generated by *in-vitro* selection techniques, namely *Systematic Evolution of Ligands by Exponential Enrichment (SELEX)* [33,34]. It shows high selectivity towards target molecules due to repetitive selection rounds, low immunogenicity, inflated stability, simple modification, and low cost [35,36]. To date, no report has been published to show the application of aptamers in MDMA detection.

One of the major aims of simultaneous detection and signal amplification is to fabricate an ultrasensitive detection platform, which nanomaterials can easily achieve. In this direction, recent studies are applying the electronic nature of zero-dimensional quantum dots (QDs) in sensing technologies [37–39]. These materials have a large surface-to-volume ratio, excellent water solubility, and abundant structural defects [39,40], which enhance their electrochemical properties. Compared to metallic QDs (e.g., CdS, CdSe, PbS, and SiQDs), carbon-based quantum dots are easy to synthesize and exhibit low toxicity with high electrochemical properties [41,42].

In the present work, we showed that N-CDs modified electrochemical sensors can be used to design an ultra-sensitive platform with high conductivity. It may provide a large surface area for MDMA-specific aptamer (here referred to as Apt_{MDMA}) to detect MDMA in biological samples. Thus, Apt_{MDMA}/N-CDs@SPE biosensor was prepared for quick, reliable, and simple detection of the recreational drug MDMA. Under optimal conditions, a low limit of detection, good linearity, and selectivity was achieved via impedimetric measurements. Moreover, a prepared sensing platform was employed for the spiked, diluted urine samples of MDMA.

2. Materials and Methods

2.1. Chemicals and reagents.

The (±)-3,4-Methylenedioxymethamphetamine solution (MDMA; 1.0 mg/ml in methanol), Amphetamine (AMP; 1.0 mg/ml in methanol), 4-Hydroxybutyric acid sodium salt solution (GHB; 1.0 mg/ml in methanol), and glutaraldehyde solution (50 wt%) were purchased from Sigma Aldrich, India. N-Ethyl-N′-(3-dimethylaminopropyl)carbodiimide (EDC), N-hydroxysuccinimide (NHS), 6-Mercapto-1-hexanol (6-MCH), potassium chloride (KCl), 2-(N-morpholino)ethanesulfonic acid (MES), ethylenediaminetetraacetic acid (EDTA), anisole, Tris, benzaldehyde, potassium hexacyanoferrate (III) ($K_3Fe(CN)_6$), and potassium ferrocyanide ($K_4Fe(CN)_6$) were procured from SRL Pvt. Ltd., India. Asprin was purchased from the local market in Noida. The mixture of EDC -NHS was prepared in 100 mM MES solution at pH 5.0 in 2:5 M ratio at room temperature (24 ± 3°C).

2.2. Apparatus and procedures.

The electrochemical studies were performed using Cyclic Voltammetry (CV), Electrochemical Impedance Spectroscopy (EIS), and Differential Pulse Voltammetry (DPV) on EC-Lab V11.10 software of Biopotentiostate workstation (BioLogic science Instrument, model no SP 200) equipped with a three-electrode cell. The physical characterization of prepared N-CDs was analyzed by Fourier-transform infrared spectroscopy (FTIR; Nicolet iS5, Thermo Scientific, India) at Amity University Uttar Pradesh (AUUP), Noida, India. The UV-vis (Shimadzu UV-2600) and Photoluminescent (PL; Ocean Optics) spectroscopy were used to determine optical characteristics at Amity University Uttar Pradesh (AUUP), Noida, India.

2.3. Synthesis of N-doped carbon dots (N-CDs).

Synthesis of N-CD nanoparticles was performed by a one-step hydrothermal process, as cited in the literature[43], with slight modification. Initially, 0.1 M polyvinylpyrrolidone (PVP) was first dissolved in distilled water and then added to a Teflon-lined stainless steel autoclave at 160 °C for 15 hours. The end solution was collected and stored at 4-8 •C in dark conditions. Prepared N-CDs were characterized with FT-IR, UV-Vis, and PL spectroscopy at AUUP, Noida, India.

2.4. Preparation of aptamer solutions.

The MDMA-specific aptamer (Apt_{MDMA}) was purchased, and HPLC was purified by Integrated DNA Technologies (IDT), USA. As shown in the sequence below, the presence of consecutive guanosine residues (underlined) confirms the presence of guanosine quadruplex for target detection. The 1.0 µM solution of aptamer was prepared in 1X TE buffer, aliquoted, and stored at 4-8 °C to be utilized within one month.

Apt_{MDMA} sequence:

5′-(HS)-$(CH_2)_6$-ACGGTTGCAAGTGGGACTCTGGTAGGCTGGGTTAATTTGG-3′ [44].

2.5. Preparation of N-CDs@SPE platform.

To improve the sensitivity of the sensor, the electrochemical property of zero-dimensional carbon dots were evaluated in our study. Electrochemical deposition of N-CDs was optimized via the electrodeposition at different time points. The chronocoulmetry (CC) was performed at -0.3 V, and N-CDs were allowed to be electrodeposited for 15, 30, 45, and 60 min. The electrodeposition of N-CD@SPE at different time points was evaluated via DPV at 100 μA, and the time point with maximum conductivity was selected for further studies.

2.6. Immobilization and characterization of Apt_{MDMA}/N-CDs.

We performed both electrochemical and optical characterization of *Apt_{MDMA}*/N-CDs in our laboratory. In the first step, N-CDs were modified with 1.0 mM cysteamine (Cys) at 4-8 °C overnight to form $–NH_2$ groups on the surface. Later, sequential treatment with 2.5% glutaraldehyde (Glu) for 1.0 hr and 2 mM EDC –5 mM NHS for 2 hrs at room temperature was performed. At last, 1.0 μM *Apt_{MDMA}* was allowed to incubate on EDC-NHS/Cys/N-CDs@SPE at 4.0 °C overnight, which was later treated with 6-MCH for 1.0 hr to elute out unbounded aptamers. The stepwise modification of *Apt_{MDMA}*/EDC-NHS/Cys/N-CDs@SPE preparation was studied by CV with potential between -0.5 V and 0.5 V at a scan rate of 100 mV/s, and EIS in a frequency range of 1.0 MHz- 500 mHz respectively. Furthermore, this sequential fabrication process was evaluated via PL spectroscopy at an excitation wavelength of 365 nm.

2.7. Optimization of working conditions for Apt_{MDMA}/N-CDs@SPE.

To determine the efficient working of *Apt_{MDMA}*/N-CDs@SPE, pH, and incubation time were optimized before further experiments. The prepared *Apt_{MDMA}*/N-CDs@SPE was allowed to incubate with MDMA at different pHs in the range of 5.0-9.0 with an incubation time of 10-60 min. The optimized values were used in further experiments.

2.8. Signal response of Apt_{MDMA}/N-CDs in the presence of MDMA.

In order to demonstrate the MDMA detection strategy, quantitative analysis was recorded by DPV at 100 μA in $K_3Fe(CN)_6/K_4Fe(CN)_6$ electrolyte and change in luminescence by PL spectroscopy at 365 nm. Various concentrations of MDMA (0.001-1.0 nM) were allowed to incubate with *Apt_{MDMA}*/N-CDs for the optimized time period, and changes in signals were recorded via DPV and PL. The *Apt_{MDMA}*/N-CDs@SPE was regenerated with 6.0 M urea at 37 °C for 15 mins after each concentration study. The limit of detection (*LOD*) was calculated based on the standard deviation of the response (*Sy*) of the curve and the slope of the calibration curve (*S*) at levels approximating the LOD according to the formula: LOD = 3.3(*Sy/S*). Furthermore, the modified electrode's selectivity was measured in the presence of GHB, aspirin, anisole, benzaldehyde, and a mixture. These samples were allowed to incubate with the modified electrode, and signal changes were recorded.

2.9. Analysis of prepared aptasensor in spiked urine samples.

The urine samples were collected from the Biodiagnostic lab., East Rohini, Delhi, India, and stored at -20°C before use. The 10 μl of MDMA was spiked into diluted urine to final concentrations of 0.1 nM, 0.3 nM, 0.7 nM, and 1.0 nM, and EIS was recorded.

3. Results and Discussion

3.1. Spectroscopic characterization of N-CDs.

The synthesized N-doped CDs were characterized by FTIR, UV-Vis, and PL spectroscopy. As shown in Figure 1, the characteristic peak of N-CDs appeared at 1281 cm^{-1} and 3396 cm^{-1}, corresponding to stretching vibrations of C-N in amides [43,45], and O-H and O-H and N-H bonds [46,47]. The high-intensity peak at 1638 cm^{-1} also confirmed C=O stretching vibration in primary and/or tertiary amides structures [43], which was previously verified by the peak at 1281 cm^{-1}. This result indicated that prepared CDs possessed an abundant amount of N-groups to improve the conducting nature of the material.

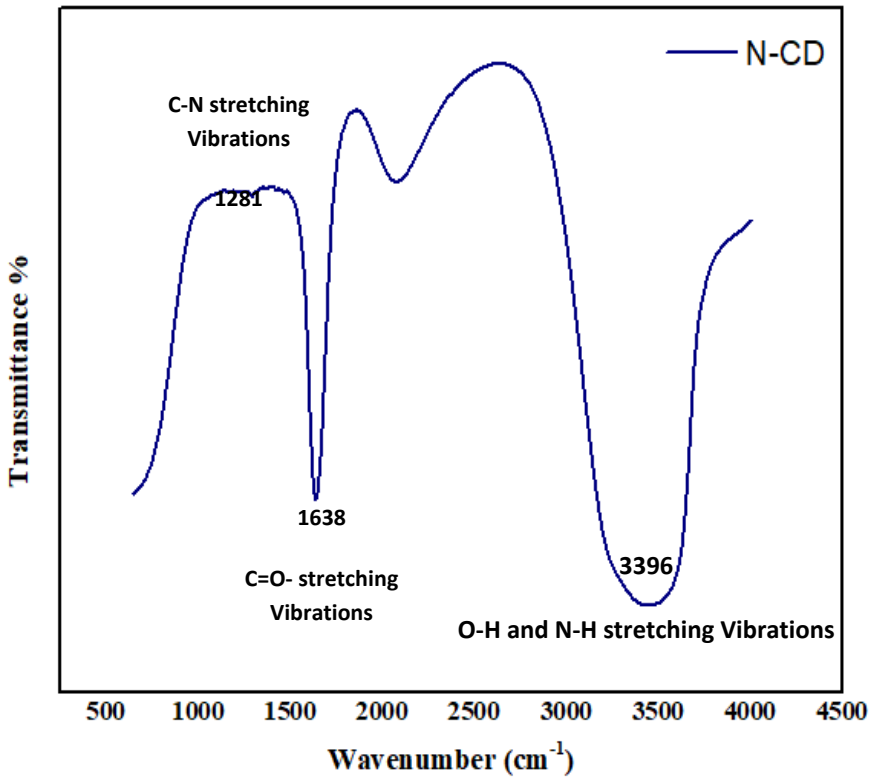

Figure 1. FT-IR spectra of prepared N-CDs in the range of 500-4000 cm^{-1}.

The UV-vis and PL spectra of the prepared N-CDs were also studied to evaluate optical properties. As shown in Figure 2(a), a flat bump near ~200-240 nm attributed to π- π* and n-π* transitions of the C-C and C=O bands of the localized sp^2 cluster in formed –COO groups of the N-CDs surface and confirmed trigonal symmetry of the material [48]. Furthermore, a peak at 453 nm and a broad spectrum of 512 nm in PL spectra (Figure 2(b)) revealed blue [49] and green emissions [48], respectively. Moreover, prepared N-CD exhibited good photostability at room temperature for one month.

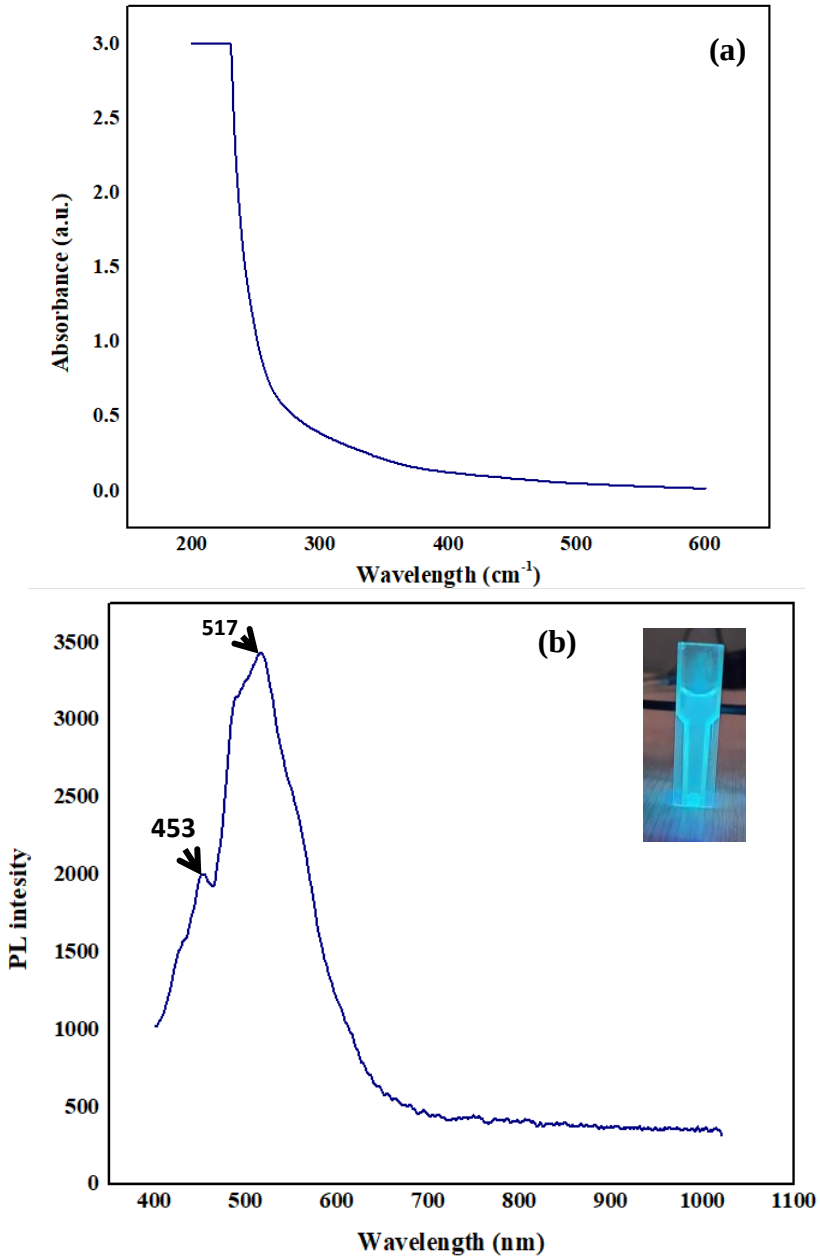

Figure 2. Spectroscopical analysis of synthesized N-CDs: **(a)** UV-Vis, and **(b)** PL spectroscopy.

3.2. Electrochemical characterization of aptasensor.

The overall development process of *Apt*$_{MDMA}$/N-CDs@SPE sensor is depicted in the graphical abstract. During each step of the aptasensor construction, the *Apt*$_{MDMA}$/N-CDs@SPE platform was characterized by cyclic voltammetry (CV) and potentiostatic electrochemical impedance spectroscopy (PEIS) measurements. Prior to recording electrochemical responses in electrode fabrication, N-CDs@SPE were measured after electrodeposition of N-CDs for 15, 30, 45, and 60 min. As illustrated in Figure 3, the DPV current peak increased from 15-45 min and then decreased. Therefore, we selected 45 min for N-CDs deposition in further study. The electrodeposition for 60 min might have caused dense surface clustering that modestly lowers electron exchange between the electrode and the solution and thus decreases the peak current.

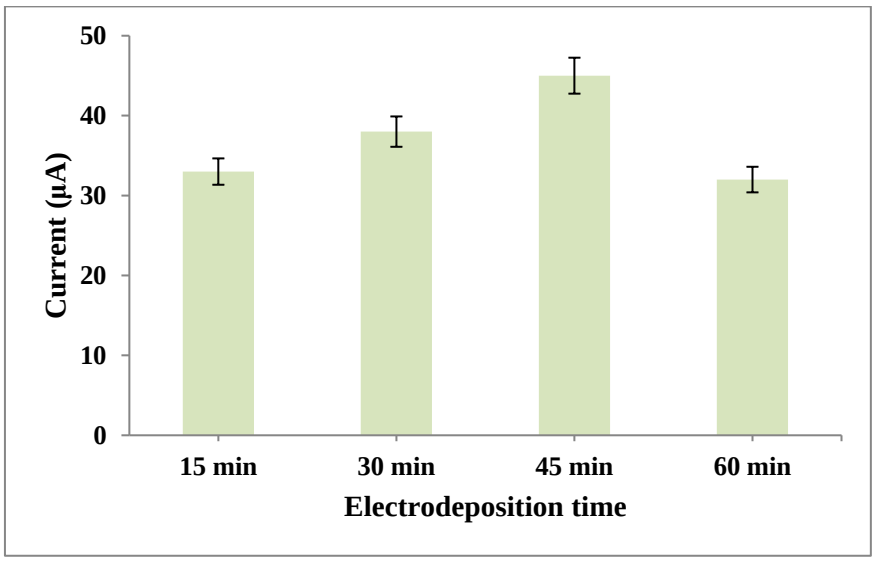

Figure 3. Optimization of N-CDs electrodeposition at 15, 30, 45, and 60 min.

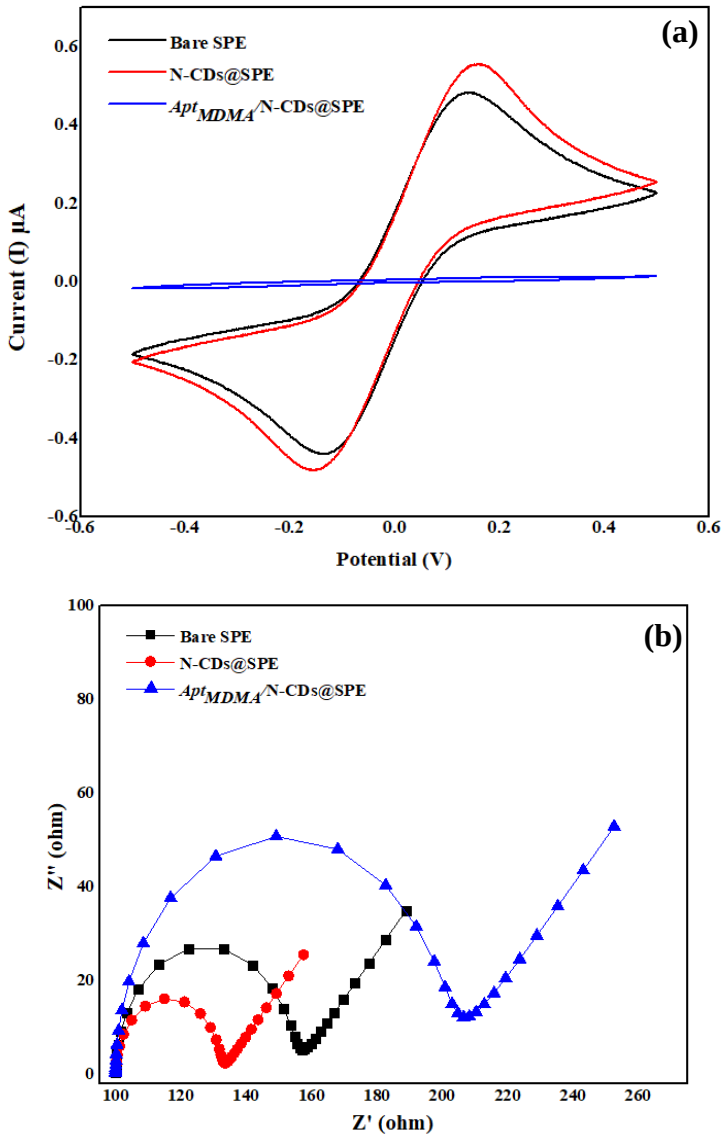

Figure 4. Electrochemical analysis of stepwise modified electrode(bare SPE, N-CDs@SPE, and Apt_{MDMA}/N-CDs@SPE. **(a)** PEIS plots of fabricated electrode for MDMA recognition in the frequency range of 1.0 MHz- 500 mHz **(b)** CV responses of the modified electrode for MDMA determination in the range of 0.05 to -0.05 V.

Furthermore, as shown in Figure 4(a), the CV characterization showed that the bare SPE allows charge transfer with typical pair of diffusional reversible peaks, as the separation of forward and reverse peak potential (ΔE_p) was >0.058 V [50,51]. Further electrodeposition of N-CDs@SPE exhibited an increase in peak current and decrease in ΔE_p, also justified improved conductivity and rise in electron transfer between modified N-CDs@SPE and redox probe [52]. After immobilization of Apt_{MDMA} onto the N-CDs@SPE surface, the platform showed a significant lowering in current which was consistent with forming a kinetic barrier between the negatively charged phosphate group of the Apt_{MDMA} and the electrolyte [53,54]. The Nyquist plots of the Apt_{MDMA}/N-CDs@SPE platform were complementary to these CV results, in which the charge transfer resistance (R_{ct}) value lowered by 23.8 ohms after N-CDs deposition and significantly increased to 206.1 after Apt_{MDMA} modification (Figure 4(b)). The higher the R_{ct} value, the higher the resistance.

3.3. Optimization of experimental conditions for the aptasensor.

To measure the efficient working of the modified electrode, it was incubated to a solution with different pH, and a variation in electrochemical signals was recorded. As shown in Figure 5, the highest impedance peaked at pH 7.4, which indicates the higher efficiency of the Apt_{MDMA}/N-CDs@SPE platform near real-world physiological pH.

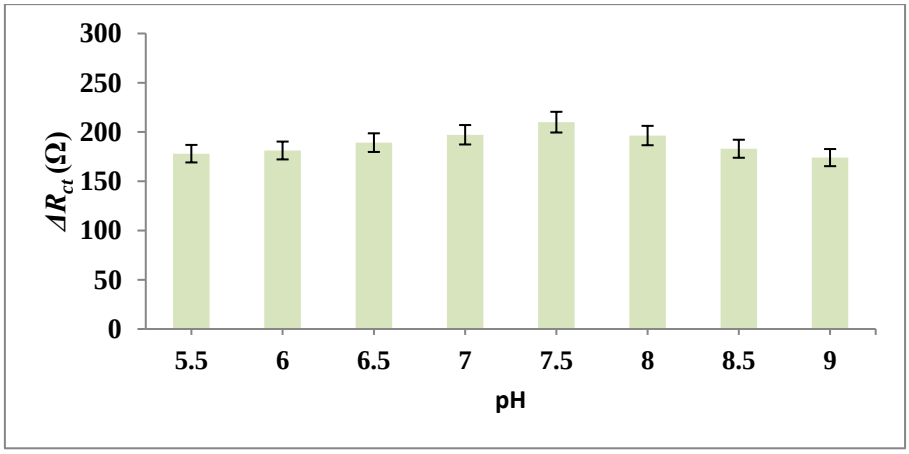

Figure 5. Effect of various pH (5.5-9.0) on the analytical performance of the aptasensor.

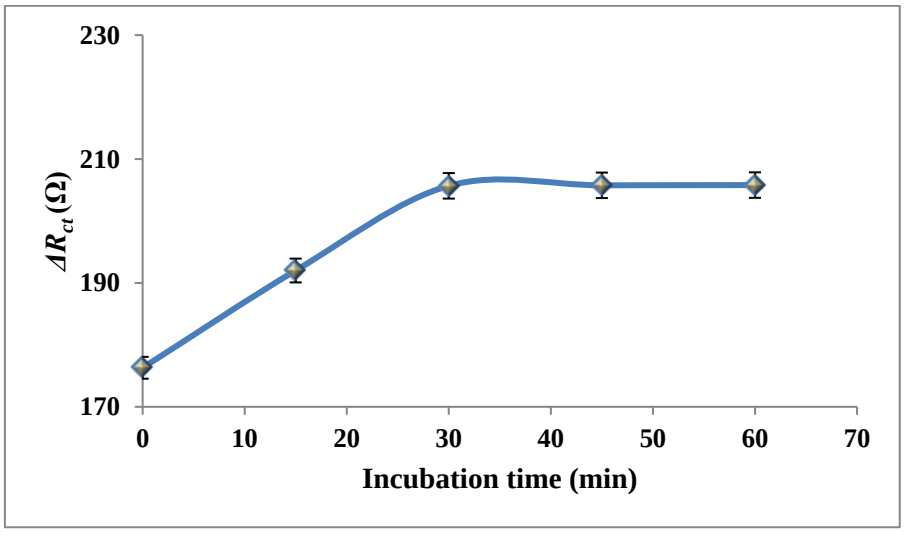

Figure 6. Trade in charge transfer resistance (ΔR_{ct}) after MDMA incubation on fabricated Apt_{MDMA}/N-CDs@SPE electrode (0, 15, 30, 45, and 60 min).

The incubation time of the fabricated Apt_{MDMA}/N-CDs@SPE electrode was evaluated by incubating MDMA with the electrode for 0-60 min with a time gap of 15 min. As shown in Figure 6, the ΔR_{ct} values escalated from 0 to 30 min and became constant. Therefore, we choose 30 min as the optimum incubation time in the present study.

3.4. Quantitative detection of MDMA.

The PEIS analysis was evaluated against a series of MDMA concentrations in the range of 1.0 pM to 1.0 nM on the modified Apt_{MDMA}/N-CDs@SPE platform. The concentration-dependent elevation in R_{ct} values was reported in PEIS graph (Figure 7(a)), which indicated specific interaction between Apt_{MDMA} and the target. It changes mass and electron transfer on the surface, affecting the system's resistance [55,56]. To evaluate the effect of different concentrations of MDMA on the fabricated electrode, a calibration curve between ΔR_{ct} and MDMA concentrations was plotted, where $\Delta R_{ct} = R_{ct,\ MDMA} - R_{ct,\ aptamer}$ (Figure 7(b)). It derived a linear regression equation (eq. 1) with a slope of 184.7 Ω/ nM and a y-intercept of 33.85 Ω with R^2 of 0.991. The LOD of the sensor was calculated as 0.18 nM with a sensitivity of 0.36 Ω/ nM.

$$\Delta R_{ct}\,(\Omega) = 184.7(\Omega/\text{nM})\cdot\text{MDMA conc. (nM)}] + 33.85\ (\Omega) \quad (R^2 = 0.991) \qquad (1)$$

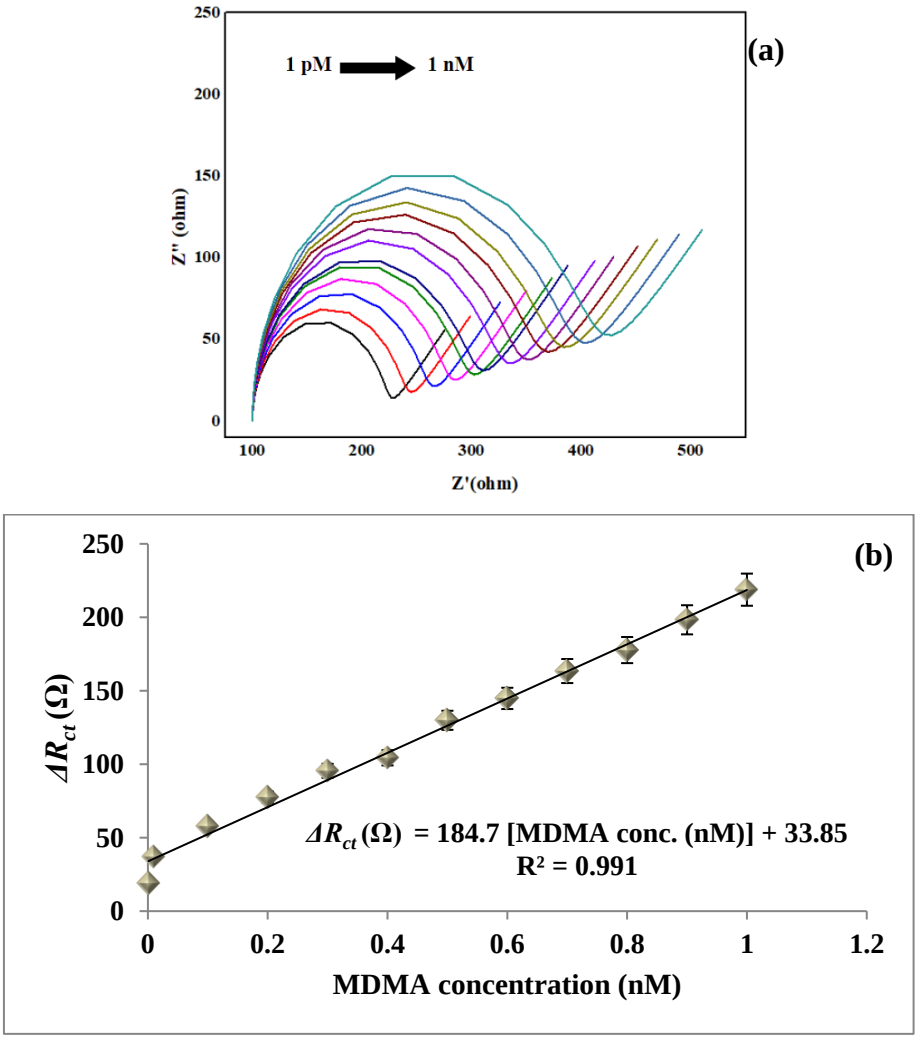

Figure 7. Analysis of Apt_{MDMA}/N-CDs@Au modified platform at various MDMA concentrations. **(a)** Change in charge transfer resistance (ΔR_{ct}) at different MDMA concentrations (0.001, 0.01, 0.1, 0.2, 0.3, 0.4, 0.5, 0.6, 0.7, 0.8, 0.9, and 1.0 nM). **(b)** Calibration curve between ΔR_{ct} and individual MDMA concentrations.

Additionally, the effect of different concentrations of MDMA on developed aptasensor was also evaluated by PL spectroscopy, and diminishing fluorescence was observed. As shown in Figure 8, with increasing MDMA concentration from 10 pM to 1.0 nM, the PL intensity peaks decrease and confirm the target's binding with the sensor.

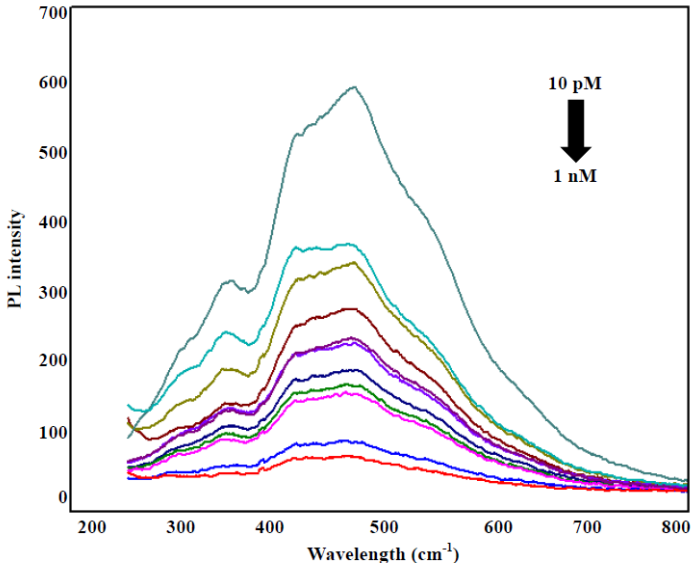

Figure 8. Change in PL intensity at different concentrations of MDMA (10 pM-1 nM).

3.5. Scan rate and selectivity.

To determine the electrochemical mechanism of the prepared aptasensor, the relationship between scan rate and redox peak currents was established. As shown in Figure 9(a), with an increase in √scan rate from 20 to 100 mV/s, there was an increase in peak currents of the voltammograms in the presence of 0.18 nM MDMA. The linear calibration curve between redox peak current (I) and √scan rate (Figure 9(b)) also confirmed that our electrochemical process is diffusion controlled. However, a scan rate of 50 mV/s was elected as the optimum scan rate to maintain the high sensitivity while lessening the background noise of the current. The association between current and scan rate can be presented as:

$$\text{Ipa (biocathodic)} = -0.001\ (\sqrt{\text{scan rate}}) + 0.019\ (R^2 = 0.958) \quad (2)$$

$$\text{Ipc (bioanodic)} = 0.001\ (\sqrt{\text{scan rate}}) - 0.031\ (R^2 = 0.996) \quad (3)$$

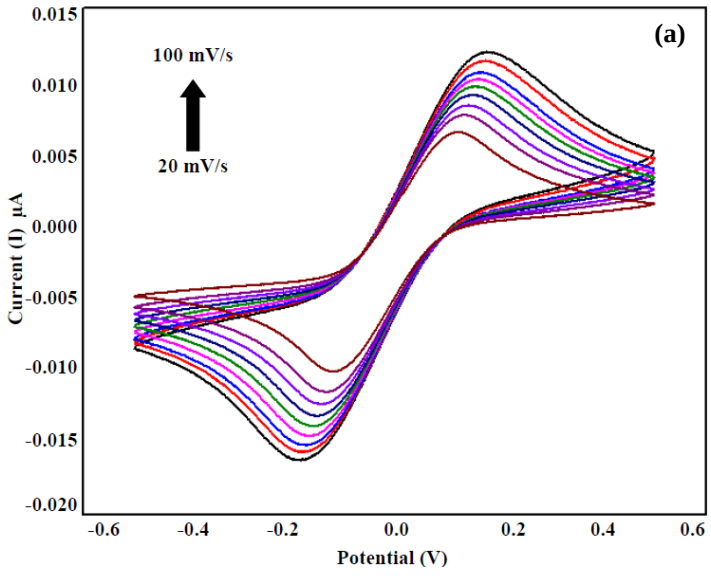

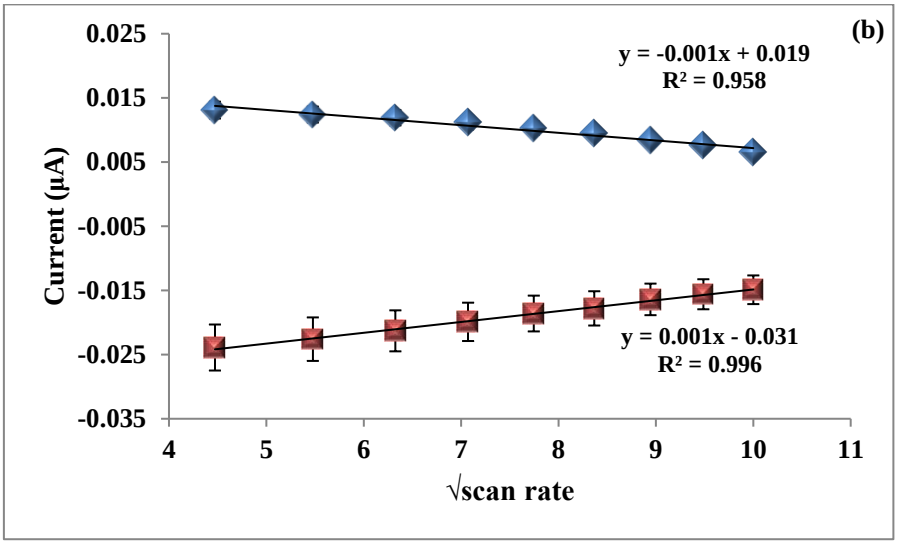

Figure 9. Evaluation of redox mechanism of aptasensor in the presence of 0.18 nM MDMA: **(a)** CV curves illustrations at scan rates in the range of 20, 30, 40, 50, 60, 70, 80, 90, and 100 mV/s. **(b)** Calibration curves of √scan rate vs. redox current peak.

To analyze the selectivity of the developed aptasensor, the *Apt*$_{MDMA}$/N-CDs@SPE electrode was challenged with 0.18 nM concentration of MDMA and other interferents GHB, aspirin, anisole, benzaldehyde (BA), and mixture. As illustrated in Fig. 10, these interferents did not significantly disrupt the electrochemical responses compared to the result derived from MDMA incubation. Thus, justify the higher selectivity of the developed sensing device.

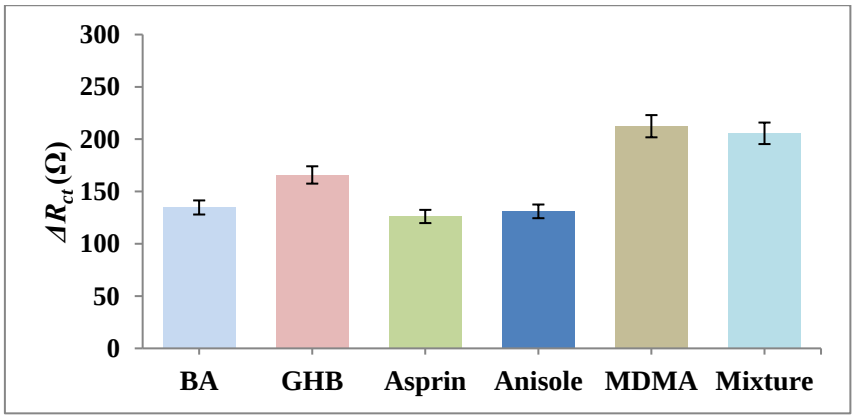

Figure 10. Selectivity of developed aptasensor in the presence of 0.18 nM MDMA, BA, 4-GHB, aspirin, anisole, benzaldehyde, and the mixture of the interferents.

3.6. Real sample analysis.

To evaluate to the applicability of the developed aptasensor, different concentration of MDMA in human spiked urine samples was determined. The electrochemical signals of MDMA concentration of 0.1, 0.4, 0.7, or 1.0 nM spiked samples exhibited recovery in the range of 88-92% (Table 1), indicating good accuracy and excellent potential for practical application in analytical chemistry.

Table 1. Comparative analysis of previously designed electrochemical sensors for MDMA recognition.

SN	Sensor type	Sensing mechanism	LOD	Linear range	Sample type
1)	Graphite-based sensor [57]	DPV	40 µM	500 – 4980 µM	PBS buffer
2)	Gold sensing platform [58]	SWV	*NR	110.9–258.9 µM	Urine

SN	Sensor type	Sensing mechanism	LOD	Linear range	Sample type
3)	Microcantilever immunosensor [59]	Frequency shift	5.0×10^3 μM	5.0×10^3 - 50×10^3 μM	*NR
4)	CB[6]based sensor [19]	CV	Dip-coating: 3.5 μM and spin-coating: 2.7 μM	4.2×10^{-3} - 4.8×10^{-2} μM	*NR
5)	MIP based sensor [23]	SWV	0.7 μM	2.5-200 μM	Serum and urine
6)	N-CDs quantum dots based Aptasensor [Present study]	PEIS	0.18 nM	0.01-1.0 nM	Diluted urine

*NR-Not reported

Table 1 has confirmed that the developed aptasensor in the current study showed a significant difference in electrochemical signals for MDMA detection, and N-CDs enhanced the electroconductivity-based sensitivity of the platform as expected. The designed aptasensor was also validated with spiked, diluted urine samples at MDMA concentrations of 0.1, 0.4, 0.7, and 1.0 nM,=as shown in Table 2.

Table 2. Determination of Apt_{MDMA}/N-CDs@SPE based sensing system for MDMA detection in spiked urine samples.

Sample	Added MDMA Conc. (nM)	Observed MDMA conc. (nM)	Recovery %
Urine	0.0	Not detectable	0.0
	0.1	0.092	92%
	0.4	0.352	88%
	0.7	0.64	91.4%
	1.0	0.91	91%

4. Conclusions

The current work proposes elegant label-free electrochemical sensing technology for MDMA detection using anti-MDMA aptamer-modified SPE. Applying highly selective aptamers-based electro-oxidation signals obtained after the MDMA recognition event allowed us to obtain a selective (negligible interference) and highly sensitive (detection at pM levels) aptasensor. With a LOD of 0.18 nM in the linear range of 0.01-1.0 nM, our aptasensor showed applicability for the trace of MDMA quantifications in urine samples.

Funding

The work is financially supported through an Extramural Research grant (File No. EMR/2016/007564) by the Science and Engineering Research Board (SERB), Government of India; Technology Development Program (TDP) (File No. TDP/BDTD/33/2019), Department of Science and Technology (DST), Government of India..

Acknowledgments

Not applicable.

Conflicts of Interest

The authors declare no conflict of interest.

References

1. Preuss, C.V.; Kalava, A.; King, K.C. Prescription of Controlled Substances: Benefits and Risks. **2018**, https://www.ncbi.nlm.nih.gov/books/NBK537318/.
2. Freudenmann, R.W.; Öxler, F.; Bernschneider-Reif, S. The origin of MDMA (ecstasy) revisited: the true story reconstructed from the original documents. *Addiction* **2006**, *101*, 1241–5, https://doi.org/10.1111/j.1360-0443.2006.01511.x.
3. Hurst, T. World Drug Report. Encycl. *Women Crime*, Hoboken, NJ, USA: John Wiley & Sons, Inc.; **2019**, p. 1–2, https://onlinelibrary.wiley.com/doi/abs/10.1002/9781118929803.ewac0543.
4. Drug market trends: cocaine amphetaminetype stimulants. *World Drug Rep* **2021.**https://www.unodc.org/res/wdr2021/field/WDR21_Booklet_4.pdf.
5. Yazar-Klosinski B.; Mithoefer, M. Potential Psychiatric Uses for MDMA. *Clinical Pharmacology & Therapeutics* **2017**, *101*, 194–6,https://doi.org/10.1002/cpt.565.
6. Ben Hamida, S.; Lecourtier, L.; Loureiro, M.; Cosquer, B.; Tracqui, A.; Simmoneaux, V.;Nehlig, A.; Jones, B.C.; Pereira de Vasconcelos, A.; Cassel, J.C. Ventral striatum regulates behavioral response to ethanol and MDMA combination. *Addiction Biology* **2021**, *26*, e12938,https://doi.org/10.1111/adb.12938.
7. Dolder, P.C.; Müller, F.; Schmid, Y.; Borgwardt, S.J.; Liechti, M.E. Direct comparison of the acute subjective, emotional, autonomic, and endocrine effects of MDMA, methylphenidate, and modafinil in healthy subjects. *Psychopharmacology(Berl)* **2018**, *235*, 467–79, https://doi.org/10.1007/s00213-017-4650-5.
8. Leung, K.W.; Wong, Z.C.; Ho, J.Y.; Yip, A.W.; Cheung, J.K.; Ho, K.K.; Duan, R.; Tsim, K.W. Surveillance of drug abuse in Hong Kong by hair analysis using LC-MS/MS. *Drug Test Anal.* **2018**, *10*, 977–83. https://doi.org/10.1002/dta.2345.
9. Naqi, H.A.; Husbands, S.M.; Blagbrough, I.S. 1 H quantitative NMR and UHPLC-MS analysis of seized MDMA/NPS mixtures and tablets from night-club venues. *Anal Methods* **2019**, *11*, 4795–807, https://doi.org/10.1039/C9AY01403A.
10. Di Rago, M.; Chu, M.; Rodda, L.N.; Jenkins, E.; Kotsos. A.; Gerostamoulos, D. Ultra-rapid targeted analysis of 40 drugs of abuse in oral fluid by LC-MS/MS using carbon-13 isotopes of methamphetamine and MDMA to reduce detector saturation. *Analytical and Bioanalytical Chemistry* **2016**, *408*, 3737–49. https://doi.org/10.1007/s00216-016-9458-3.
11. Duarte, L.O.; Ferreira, B.; Silva, G.R.; Ipólito, A.J.; de Oliveira, M.F. Validated green phenyl reversed-phase LC method using ethanol to determine MDMA in seized ecstasy tablets. *Journal of Liquid Chromatography and Related Technologies* **2020**, *43*, 761–9, https://doi.org/10.1080/10826076.2020.1811725.
12. Jain, U.; Saxena, K. Smart Nanobiosensors. In:*Nanosensors for Smart Manufacturing* **2021**,*2021*, p. 231–45, https://doi.org/10.1016/B978-0-12-823358-0.00012-5.
13. Jain, U.; Soni, S.; Balhara, Y.P.S.; Khanuja, M.; Chauhan, N. Dual-Layered Nanomaterial-Based Molecular Pattering on Polymer Surface Biomimetic Impedimetric Sensing of a Bliss Molecule, Anandamide Neurotransmitter. *ACS Omega* **2020**, 5, *19*, 10750-10758,https://doi.org/10.1021/acsomega.0c00285.
14. Chauhan, N.; Soni, S.; Agrawal, P.; Balhara, Y.P.S.; Jain, U. Recent advancement in nanosensors for neurotransmitters detection: Present and future perspective. *Process Biochemistry* **2020**, *91*, 241–59,https://doi.org/10.1016/j.procbio.2019.12.016.
15. Chauhan, N.; Saxena, K.; Tikadar, M.; Jain, U. Recent advances in the design of biosensors based on novel nanomaterials: An insight. *Nanotechnology and Precision Engineering.* **2021**, *4*, 045003, https://doi.org/10.1063/10.0006524.
16. Chauhan, N.; Soni, S.; Jain, U. Optimizing testing regimes for the detection of {COVID}-19 in children and older adults. *Expert Review of Molecular Diagnostics* **2021**, *21*, 999-1016,https://doi.org/10.1080/14737159.2021.1962708.
17. Soni, S.; Jain, U.; Chauhan, N. A systematic review on sensing techniques for drug- facilitated sexual assaults (DFSA) monitoring. *Chinese Journal of Analytical Chemistry* **2021**, *49*, 11, 83-92, https://doi.org/10.1016/j.cjac.2021.09.001.
18. Balayan, S.; Chauhan, N.; Chandra, R.; Jain, U. Electrochemical Based C-Reactive Protein (CRP) Sensing Through Molecularly Imprinted Polymer (MIP) Pore Structure Coupled with Bi-Metallic Tuned Screen-Printed Electrode. *Biointerface Research in Applied Chemistry* **2021**, *12*,7697–714, https://doi.org/10.33263/BRIAC126.76977714.

19. Tadini, M.C.; Balbino, M.A.; Eleoterio, I.C.; de Oliveira, L.S.; Dias, L.G.; Jean-François Demets, G.; de Oliveira, M.F. Developing electrodes chemically modified with cucurbit[6]uril to detect 3,4-methylenedioxymethamphetamine (MDMA) by voltammetry. *Electrochimica Acta***2014**, *121*, 188–93, https://doi.org/10.1016/j.electacta.2013.12.107.
20. Lagona, J.; Mukhopadhyay, P.; Chakrabarti, S.; Isaacs, L. The Cucurbit[n]uril Family. *Angewandte Chemie International Edition* **2005**, *44*, 4844-70, https://doi.org/10.1002/anie.200460675.
21. Liu, L.; Zhao, N.; Scherman, O.A. Ionic liquids as novel guests for cucurbit[6]uril in neutral water. *Chemical Communications* **2008**, *9*, 1070-1072, https://doi.org/10.1039/B716889F.
22. Zhang, R.; Fu, K.; Zou, F.; Bai, H.; Zhang, G.; Liang, F.; Liu, Q. Highly sensitive electrochemical sensor based on Pt nanoparticles/carbon nanohorns for simultaneous determination of morphine and MDMA in biological samples. *Electrochimica Acta* **2021**, *370*, 137803, https://doi.org/10.1016/j.electacta.2021.137803.
23. Couto, R.A.; Costa, S.S.; Mounssef Jr, B.; Pacheco, J.G.; Fernandes, E.; Carvalho, F.; Rodrigues, C.M.; Delerue-Matos, C.; Braga, A.A.; Goncalves, L.M.; Quinaz, M.B. Electrochemical sensing of ecstasy with electropolymerized molecularly imprinted poly(o-phenylenediamine) polymer on the surface of disposable screen-printed carbon electrodes. *Sensors Actuators B: Chemical* **2019**, *290*, 378–86, https://doi.org/10.1016/j.snb.2019.03.138.
24. Zhang, D.W.; Zhang, F.T.; Cui, Y.R.; Deng, Q.P.; Krause, S.; Zhou, Y.L.; Zhang, X.X. A label-free aptasensor for the sensitive and specific detection of cocaine using supramolecular aptamer fragments/target complex by electrochemical impedance spectroscopy. *Talanta* **2012**, *92*, 65–71,https://doi.org/10.1016/j.talanta.2012.01.049.
25. Roushani, M.; Shahdost-fard, F. A novel ultrasensitive aptasensor based on silver nanoparticles measured via enhanced voltammetric response of electrochemical reduction of riboflavin as redox probe for cocaine detection. *Sensors Actuators B: Chemical* **2015**, *207*, 764–71,https://doi.org/10.1016/j.snb.2014.10.131.
26. Khosropour, H.; Rezaei, B.; Alinajafi, H.A.; Ensafi, A.A. Electrochemical sensor based on glassy carbon electrode modified by polymelamine formaldehyde/graphene oxide nanocomposite for ultrasensitive detection of oxycodone. *Microchimica Acta* **2021**, *188*, 1,https://doi.org/10.1007/s00604-020-04655-3.
27. Hedayati, N.; Taghdisi, S.M.; Yazdian-Robati, R.; Mansouri, A.; Abnous, K.; Ahmad Mohajeri, S. Selection of DNA aptamers for tramadol through the systematic evolution of ligands by exponential enrichment method for fabrication of a sensitive fluorescent aptasensor based on graphene oxide. *Spectrochimica Acta Part A: Molecular and Biomolecular Spectroscopy* **2021**, *259*, 119840, https://doi.org/10.1016/j.saa.2021.119840.
28. Wang, X.; Dong, S.; Gai, P.; Duan, R.; Li, F. Advances in Gold Nanoparticles-Based Colorimetric Aptasensors for the Detection of Antibiotics: An Overview of the Past Decade. *Nanomaterials* **2021**, *11*, 840, https://doi.org/10.3390/nano11040840.
29. Birader, K.; Kumar, P.; Tammineni, Y.; Barla, J.A.; Reddy, S.; Suman, P. Colorimetric aptasensor for on-site detection of oxytetracycline antibiotic in milk. *Food Chemistry* **2021**, *356*, 129659, https://doi.org/10.1016/j.foodchem.2019.125377.
30. Peng, B.; Zhang, Z.; Tang, L.; Ouyang, X.; Zhu, X.; Chen, L.; Fan, X.; Zhou, Z.; Wang, J. Self-Powered Photoelectrochemical Aptasensor for Oxytetracycline Cathodic Detection Based on a Dual Z-Scheme WO_3/g-C_3N_4/MnO_2 Photoanode. *Analytical Chemistry* **2021,** *93*, 9129-38, https://doi.org/10.1021/acs.analchem.1c00929.
31. Salandari-Jolge, N.; Ensafi, A.A.; Rezaei B. Ultra-sensitive electrochemical aptasensor based on zeolitic imidazolate framework-8 derived Ag/Au core-shell nanoparticles for mercury detection in water samples. *Sensors Actuators B: Chemical* **2021***331*, 129426, https://doi.org/10.1016/j.snb.2020.129426.
32. Guo, W.; Zhang, C.; Ma, T.; Liu, X.; Chen, Z.; Li, S.; Deng, Y. Advances in aptamer screening and aptasensors'detection of heavy metal ions. *Journal of Nanobiotechnology* **2021**, *19*, 1-9, https://doi.org/10.1039/C5NR04532K.
33. Komarova, N.; Kuznetsov, A. Inside the Black Box: What Makes SELEX Better? *Molecules* **2019**, *24*, 3598,https://doi.org/10.3390/molecules24193598
34. Calzada, V. Aptamers in Diagnostic and Molecular Imaging Applications. In: *Aptamers in Biotechnology*, Scheper, T.; editor, Springer; **2019**. https://doi.org/10.1007/10_2019_115.
35. Huang, J.; Chen, X.; Fu, X.;Li, Z.; Huang, Y.; Liang, C. Advances in aptamer-based biomarker discovery. *Frontiers in Cell and Developmental Biology* **2021,** *9*, 571, https://doi.org/10.3389/fcell.2021.659760.
36. Chen, A; Yang, S. Replacing antibodies with aptamers in lateral flow immunoassay. *Biosensors Bioelectronics* **2015**, *71*, 230–42, https://doi.org/10.1016/j.bios.2015.04.041.

37. Pareek, S.; Rout, V.; Jain, U.; Bharadwaj, M.; Chauhan, N. Nitrogen-Doped Carbon Dots for Selective and Rapid Gene Detection of Human Papillomavirus Causing Cervical Cancer. *ACS Omega* **2021**, *6*, 31037–45,https://doi.org/10.1021/acsomega.1c03919.
38. Yu, H.W.; Zhang, Z.; Jiang, J.H.; Pan, H.Z.; Chang, D. Simple strategy for sensitive detection of dopamine using CdTe QDs modified glassy carbon electrode. *Journal of Clinical Laboratory Analysis* **2018**, *32*, e22320. https://doi.org/10.1002/jcla.22320.
39. Yola, M.L.; Atar, N. A novel detection approach for serotonin by graphene quantum dots/two-dimensional (2D) hexagonal boron nitride nanosheets with molecularly imprinted polymer. *Applied Surface Science* **2018**, *458*, 648–55,https://doi.org/10.1016/j.apsusc.2018.07.142.
40. Li, Y.; Han, M.; Bai, H.; Wu, Y.; Dai, Z.; Bao, J. A sensitive electrochemical aptasensor based on water soluble CdSe quantum dots (QDs) for thrombin determination. *Electrochimica Acta* **2011**, *56*, 7058–63,https://doi.org/10.1016/j.electacta.2011.05.119.
41. Huang, Q.; Lin, X.; Tong, L.; Tong, Q.X. Graphene Quantum Dots/Multiwalled Carbon Nanotubes Composite-Based Electrochemical Sensor for Detecting Dopamine Release from Living Cells. *ACS Sustainable Chemistry & Engineering* **2020**, *8*, 1644–50, https://doi.org/10.1021/acssuschemeng.9b06623.
42. Liu, Y.; Cao, N.; Gui, W.; Ma, Q. Nitrogen-doped graphene quantum dots-based fluorescence molecularly imprinted sensor for thiacloprid detection. *Talanta* **2018**, *183*, 339–44,https://doi.org/10.1016/j.talanta.2018.01.063.
43. Travlou, N.A, Giannakoudakis, D.A.; Algarra, M.; Labella, A.M.; Rodríguez-Castellón, E.; Bandosz, T.J. S- and N-doped carbon quantum dots: Surface chemistry dependent antibacterial activity. *Carbon NY* **2018**, *135*, 104–11,https://doi.org/10.1016/j.carbon.2018.04.018.
44. Shi, Q.; Shi, Y.; Pan, Y.; Yue, Z.; Zhang, H.; Yi, C. Colorimetric and bare eye determination of urinary methylamphetamine based on the use of aptamers and the salt-induced aggregation of unmodified gold nanoparticles. *Microchimica Acta* **2015**, *182*, 505–11,https://doi.org/10.1007/s00604-014-1349-8.
45. Su, Y.; Zhou, X.; Long, Y.; Li, W. Immobilization of horseradish peroxidase on amino-functionalized carbon dots for the sensitive detection of hydrogen peroxide. *Microchimica Acta* **2018**, *185*, 114, https://doi.org/10.1007/s00604-017-2629-x.
46. Xie, C.; Liu, H. Green Hydrothermal Synthesis of N-doped Carbon Dots from Biomass Highland Barley for the Detection of Hg^{2+}. *Sensors*. **2019**, *19*, 3169, https://doi.org/10.3390/s19143169.
47. Zhao, X.; Zhang, J.; Shi, L.; Xian, M.; Dong, C.; Shuang, S. Folic acid-conjugated carbon dots as green fluorescent probes based on cellular targeting imaging for recognizing cancer cells. *RSC Advances* **2017**, *7*, 42159–67, https://doi.org/10.1039/C7RA07002K.
48. Shi, L.; Chang, D.; Zhang, G.; Zhang, C.; Zhang, Y.; Dong, C.;Chu, L.; Shuang, S. Co^{2+} detection, cell imaging, and temperature sensing based on excitation-independent green-fluorescent N-doped carbon dots. *RSC Advances* **2019**, *9*, 41361–7,https://doi.org/10.1039/C9RA09405A.
49. Hu, Y.; Yang, J.; Tian, J.; Yu, J-S. How do nitrogen-doped carbon dots generate from molecular precursors? An investigation of the formation mechanism and a solution-based large-scale synthesis. *Journal of Materials Chemistry B* **2015**, *3*, 5608–14,https://doi.org/10.1039/C5TB01005E.
50. Elgrishi, N.; Rountree, K.J.; McCarthy, B.D.; Rountree, E.S.; Eisenhart, T.T.; Dempsey, J.L. A Practical Beginner's Guide to Cyclic Voltammetry. *Journal of Chemical Education* **2018**, *95*, 197–206, https://doi.org/10.1021/acs.jchemed.7b00361.
51. Analytical Electrochemistry: The Basic Concepts. (Accessed on 18 April, 2022) https://chem.libretexts.org/Bookshelves/Analytical_Chemistry/Supplemental_Modules_(Analytical_Chemistry)/Analytical_Sciences_Digital_Library/JASDL/Courseware/Analytical_Electrochemistry%3A_The_Basic_Concepts.
52. Chen, Z.; Li, L.; Zhao, H.; Guo, L.; Mu, X. Electrochemical impedance spectroscopy detection of lysozyme based on electrodeposited gold nanoparticles. *Talanta* **2011**, *83*, 1501–6, https://doi.org/10.1016/j.talanta.2010.11.042.
53. Florea, A.; Cowen, T.; Piletsky, S.; De Wael, K. Electrochemical sensing of cocaine in real samples based on electrodeposited biomimetic affinity ligands. *Analyst*. **2019**. https://doi.org/10.1039/c9an00618d.
54. Roushani, M.; Shahdost-fard, F. Impedimetric detection of cocaine by using an aptamer attached to a screen printed electrode modified with a dendrimer/silver nanoparticle nanocomposite. *Microchimica Acta* **2018**, *185*, 214,https://doi.org/10.1007/s00604-018-2709-6.

55. Zhao, Y.; Liu, H.; Shi, L.; Zheng, W.; Jing, X. Electroactive Cu_2O nanoparticles and Ag nanoparticles driven ratiometric electrochemical aptasensor for prostate specific antigen detection. *Sensors Actuators :B Chemical* **2020**, *315*, 128155, https://doi.org/10.1016/j.snb.2020.128155.
56. Hashemi, P.; Bagheri, H.; Afkhami, A.; Ardakani, Y.H.; Madrakian, T. Fabrication of a novel aptasensor based on three-dimensional reduced graphene oxide/polyaniline/gold nanoparticle composite as a novel platform for high sensitive and specific cocaine detection. *Analytica Chimica Acta* **2017**, *996*, 10–9,https://doi.org/10.1016/j.aca.2017.10.035.
57. Cumba, L.R.; Smith, J.P.; Zuway, K.Y.; Sutcliffe, O.B.; Do Carmo, D.R.; Banks, C.E. Forensic electrochemistry: Simultaneous voltammetric detection of MDMA and its fatal counterpart "dr Death"(PMA). *Analytical Methods* **2016**, *8*, 142–52,https://doi.org/10.1039/c5ay02924d.
58. Nevescanin, M.; Avramov-Ivic, M.; Petrovic, S.; Mijin.; Banovic-Stevic, S.; Jovanovic, V. The use of a gold electrode for the determination of amphetamine derivatives and application to their analysis in human urine. *Journal of the Serbian Chemical Society* **2013**, *78*, 1373–85, https://doi.org/10.2298/JSC121228032N.
59. Tseng, Y.C.; Chang, J.S.; Lin, S.; Chao, S.D.; Liu, C.H. 3,4-Methylenedioxymethylamphetamine detection using a microcantilever-based biosensor. *Sensors Actuators A Physics* **2012**, *182*, 163–7, https://doi.org/10.1016/j.sna.2012.05.036.